



Stability of HTLV-2 antisense protein is controlled by PML nuclear bodies in a SUMO-dependent manner

Louise Dubuisson^{1,2} · Florence Lormières^{1,2} · Stefania Fochi³ · Jocelyn Turpin^{1,2} · Amandine Pasquier^{1,2} · Estelle Douceron^{1,2} · Anaïs Oliva^{1,2} · Ali Bazarbachi^{4,5} · Valérie Lallemand-Breitenbach⁶ · Hugues De Thé⁶ · Chloé Journo^{1,2} · Renaud Mahieux^{1,2}

Received: 4 September 2017 / Revised: 22 December 2017 / Accepted: 29 December 2017 / Published online: 6 March 2018
© Macmillan Publishers Limited, part of Springer Nature 2018

Abstract

Since the identification of the antisense protein of HTLV-2 (APH-2) and the demonstration that APH-2 mRNA is expressed *in vivo* in most HTLV-2 carriers, much effort has been dedicated to the elucidation of similarities and/or differences between APH-2 and HBZ, the antisense protein of HTLV-1. Similar to HBZ, APH-2 negatively regulates HTLV-2 transcription. However, it does not promote cell proliferation. In contrast to HBZ, APH-2 half-life is very short. Here, we show that APH-2 is addressed to PML nuclear bodies in T-cells, as well as in different cell types. Covalent SUMOylation of APH-2 is readily detected, indicating that APH-2 might be addressed to the PML nuclear bodies in a SUMO-dependent manner. We further show that silencing of PML increases expression of APH-2, while expression of HBZ is unaffected. On the other hand, SUMO-1 overexpression leads to a specific loss of APH-2 expression that is restored upon proteasome inhibition. Furthermore, the carboxy-terminal LAGLL motif of APH-2 is responsible for both the targeting of the protein to PML nuclear bodies and its short half-life. Taken together, these observations indicate that natural APH-2 targeting to PML nuclear bodies induces proteasomal degradation of the viral protein in a SUMO-dependent manner. Hence, this study deciphers the molecular and cellular bases of APH-2 short half-life in comparison to HBZ and highlights key differences in the post-translational mechanisms that control the expression of both proteins.

These authors contributed equally: Chloé Journo and Renaud Mahieux.

Electronic supplementary material The online version of this article (<https://doi.org/10.1038/s41388-018-0163-x>) contains supplementary material, which is available to authorized users.

✉ Chloé Journo
chloe.journo@ens-lyon.fr

✉ Renaud Mahieux
renaud.mahieux@ens-lyon.fr

¹ International Center for Research in Infectiology, Retroviral Oncogenesis Laboratory, INSERM U1111 – Université Claude Bernard Lyon 1, CNRS, UMR5308, Ecole Normale Supérieure de Lyon, Université Lyon, F-69007 Lyon, France

² Equipe labellisée “Ligue Nationale Contre le Cancer”, Lyon, France

Introduction

In contrast to human T lymphotropic virus type 1 (HTLV-1) that is etiologically linked to severe diseases, such as adult T-cell lymphoma/leukemia (ATLL) and HTLV-1-associated myelopathy/tropical spastic paraparesis (HAM/TSP), infection by HTLV-2 remains asymptomatic in most infected carriers with rare cases of spinal cord disease (for a review, see [1, 2]). While HTLV-1 infects mostly CD4+ T-cells, HTLV-2 preferentially infects CD8+ T-cells [3, 4].

³ Department of Neurosciences, Biomedicine and Movement Sciences, University of Verona, Verona, Italy

⁴ Department of Internal Medicine, Faculty of Medicine, American University of Beirut, Beirut, Lebanon

⁵ Department of Anatomy, Cell Biology and Physiological Sciences, American University of Beirut, Beirut, Lebanon

⁶ Collège de France - Paris Sorbonne, Inserm U944-CNRS 7212 - Université Paris Diderot, Lettre - 11 place Marcelin Berthelot, 75231 Paris Cedex 05, France

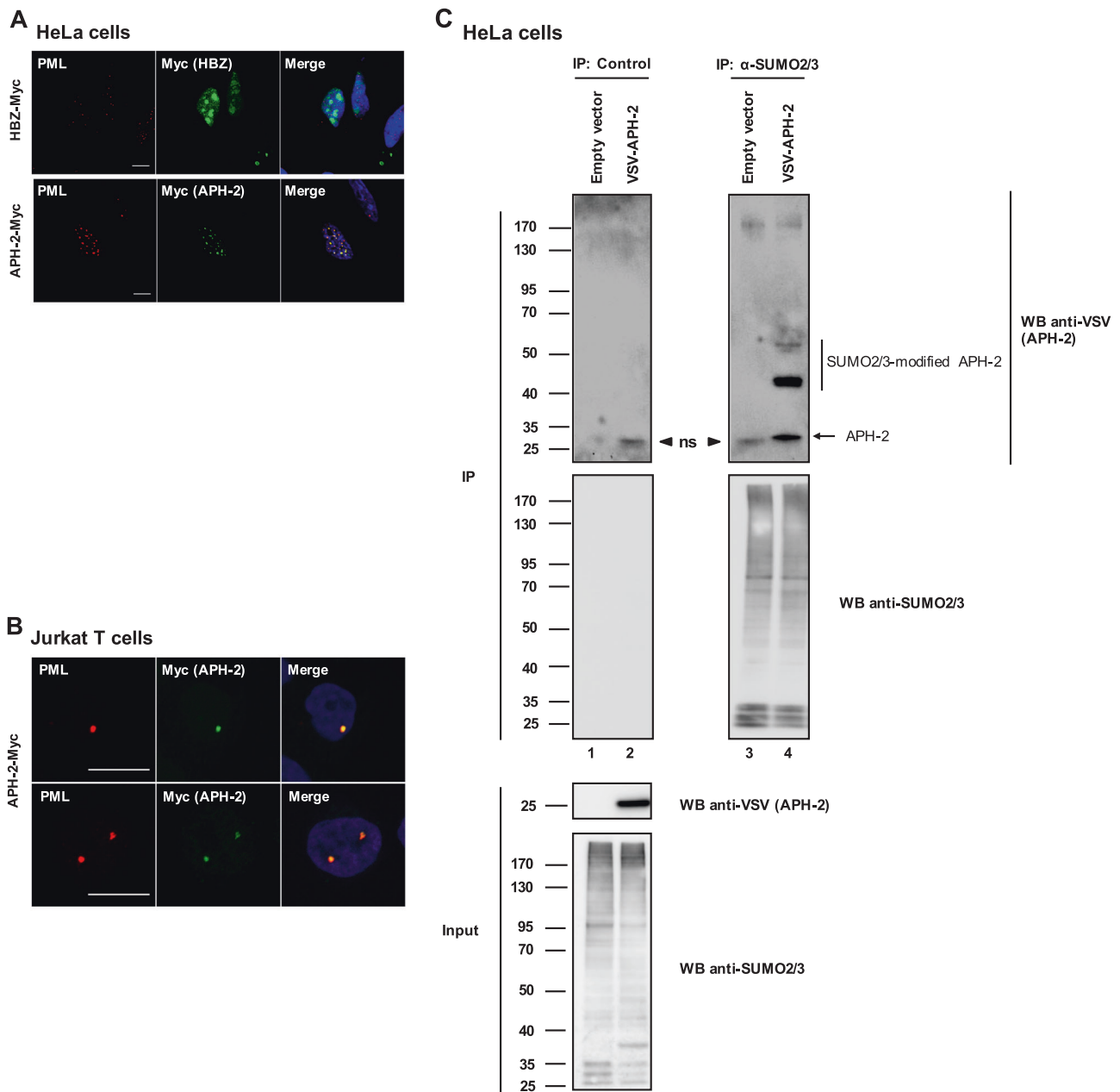


Fig. 1 APH-2 localizes in PML nuclear bodies and is SUMOylated. **a** HeLa cells and **b** Jurkat T-cells were transfected with HBZ-Myc or APH-2-Myc as indicated, and fixed 24 h after transfection. Subcellular localization of APH-2 and HBZ was examined by confocal microscopy after anti-Myc and anti-PML staining. Nuclei were counterstained with DAPI (blue). Scale bar = 10 μ m. Images representative of at least three independent experiments are shown. **c** HeLa cells were

transfected with SUMO2/3 and VSV-APH-2 or with empty vector. After treatment with MG132, anti-SUMO2/3 immunoprecipitation was performed on cell lysates in denaturing conditions, allowing specific retention of post-translationally modified APH-2. Precipitates were analyzed by western blot using anti-SUMO2/3 and anti-VSV antibodies. Results are representative of three independent experiments. *ns* non-specific signal

Because HTLV-1 and HTLV-2 share a similar genomic organization, comparative approaches meant to highlight correlations between functional properties of HTLV-1/2 genes and pathogenicity have been undertaken in the last years.

At the molecular level, HTLV-1-induced pathogenicity has been linked to the expression of two regulatory genes

encoding the transactivator Tax and the antisense protein HBZ (HTLV-1 basic leucine zipper [bZip] factor), respectively [5–7]. In addition to its viral function in transactivating the viral LTR promoter, Tax interferes with many cellular functions by interacting with cellular partners and transactivating or transrepressing cellular genes [8]. For instance, Tax induces a constitutive activation of the

canonical and non-canonical NF- κ B pathways that are involved in both cell transformation (in the course of ATLL development [9, 10]) and inflammation (in the course of HAM/TSP development [11]). As such, Tax is considered as the main viral oncoprotein. HBZ was identified in 2002 as a viral protein encoded by the negative strand of the provirus and controlled by a promoter located in the 3'LTR [12]. Of note, while *tax* expression is severely decreased and difficult to detect in most patients upon ATLL development, *hbz* spliced form (sHBZ/SP1) is consistently expressed in HTLV-1-infected asymptomatic individuals, as well as in ATLL patients. Surprisingly, HBZ-transgenic mice expressing HBZ in CD4+ T-cells, which are the main HTLV-1 target cells in vivo, also develop lymphoma and dermatitis in an IFN- γ -dependent manner [13], indicating that HBZ is intrinsically capable of inducing inflammation and cell transformation. HBZ contributes to the negative regulation of viral expression by inhibiting transcription from the 5'LTR after competition with transcription co-activators required by Tax [12]. It is now well established that HBZ cooperates with Tax for cell transformation, inflammation, and maintenance of transformed state in T-cells (for a recent review, see [14]), although Tax alone is sufficient for transforming T-cells in vitro [15] and in animal models in vivo [16, 17].

We previously reported the existence of the antisense protein of HTLV-2, termed APH-2 (ref. [18]). Similar functions have been attributed to APH-2 and HBZ regarding negative regulation of viral expression, since APH-2 is also able to inhibit transcription from HTLV-2 5'LTR [18]. However, APH-2 is unable to induce cell proliferation in vitro and is dispensable for cell immortalization in an in vivo rabbit model [19, 20]. A recent study also highlighted distinctive features of APH-2 vs. HBZ in vitro in modulating cell signaling pathways [21]. Differences in the functions of APH-2 vs. HBZ might thus contribute to the distinct ability of HTLV-2 vs. HTLV-1 to cause leukemia in vivo.

We previously observed that APH-2 had a nuclear localization that is very different from that of HBZ [18]. Importantly, APH-2 expression was also difficult to detect in vitro even in overexpression assays using expression vectors with strong promoters, indicating that the protein might be very unstable in cells. Recently indeed, Panfil et al. reported a half-life of about 30 min in transfected HEK293T cells, and of about 20 min in transfected Jurkat T-cells [21].

The aim of the present study was to understand the molecular and cellular bases of this instability in comparison to HBZ. We show here that APH-2 is covalently linked to SUMO moieties and addressed to PML nuclear bodies in all cell types tested, including T-cells. We further show that

this natural targeting of APH-2 to PML nuclear bodies induces proteasomal degradation of the viral protein in a SUMO-dependent manner. Hence, APH-2 short half-life is controlled by its post-translational modifications and its subnuclear distribution. This might explain the decreased pathogenicity of HTLV-2 viral infection.

Results

APH-2 localizes in PML nuclear bodies

We previously described APH-2 as a nuclear protein that was distributed in nuclear speckles distinct from nucleoli and which stained negative for sc-35 (ref.[18]). To further characterize APH-2 subnuclear distribution, HeLa cells were transfected with expression vectors encoding APH-2 or HBZ and sharing the same tag (Fig. 1a). As previously shown [18], confocal imaging revealed that APH-2 was distributed in nuclear speckles. Co-staining with anti-PML antibodies indicated that these speckles were PML nuclear bodies (PML-NBs) (Fig. 1a), while HBZ did not colocalize with PML, consistent with a previous report indicating that HBZ is a nucleolar protein [22].

To extend these results to T-cells, the main in vivo target of HTLV-2, Jurkat cells were transfected with an APH-2 expression vector and stained for PML (Fig. 1b). APH-2 also co-localized with PML in T-cell nuclei, confirming that this localization is not cell-type specific. To exclude the fact that these results were due to the tag used, experiments were also repeated with expression vectors containing different tags and showed the same pattern (data not shown).

We then hypothesized that APH-2 might be addressed to PML-NBs following covalent poly-SUMOylation, which may be in the form of poly-SUMO2/3 chains terminated by SUMO-1 moieties. Therefore, SUMO2/3 was immunoprecipitated from cells co-transfected with APH-2 and SUMO2/3 vectors. Those cells were treated with the MG132 proteasome inhibitor to facilitate APH-2 detection (Fig. 1c). Immunoprecipitation was performed under denaturing conditions to eliminate non-covalent partners. Purification of SUMO2/3 followed by anti-VSV-APH-2 western blot led to the detection of two SUMO2/3-modified forms of APH-2 that were enriched compared to empty vector-transfected cells (Fig. 1c compare lane 3 vs. 4). These results are typical of SUMO-modified proteins. Complementary experiments also indicated that APH-2 is modified by SUMO1 (Supplemental Fig. 1). Thus, APH-2 is SUMOylated in cells. Taken together, these observations suggest that SUMOylated APH-2 could be addressed to PML-NBs where it accumulates.

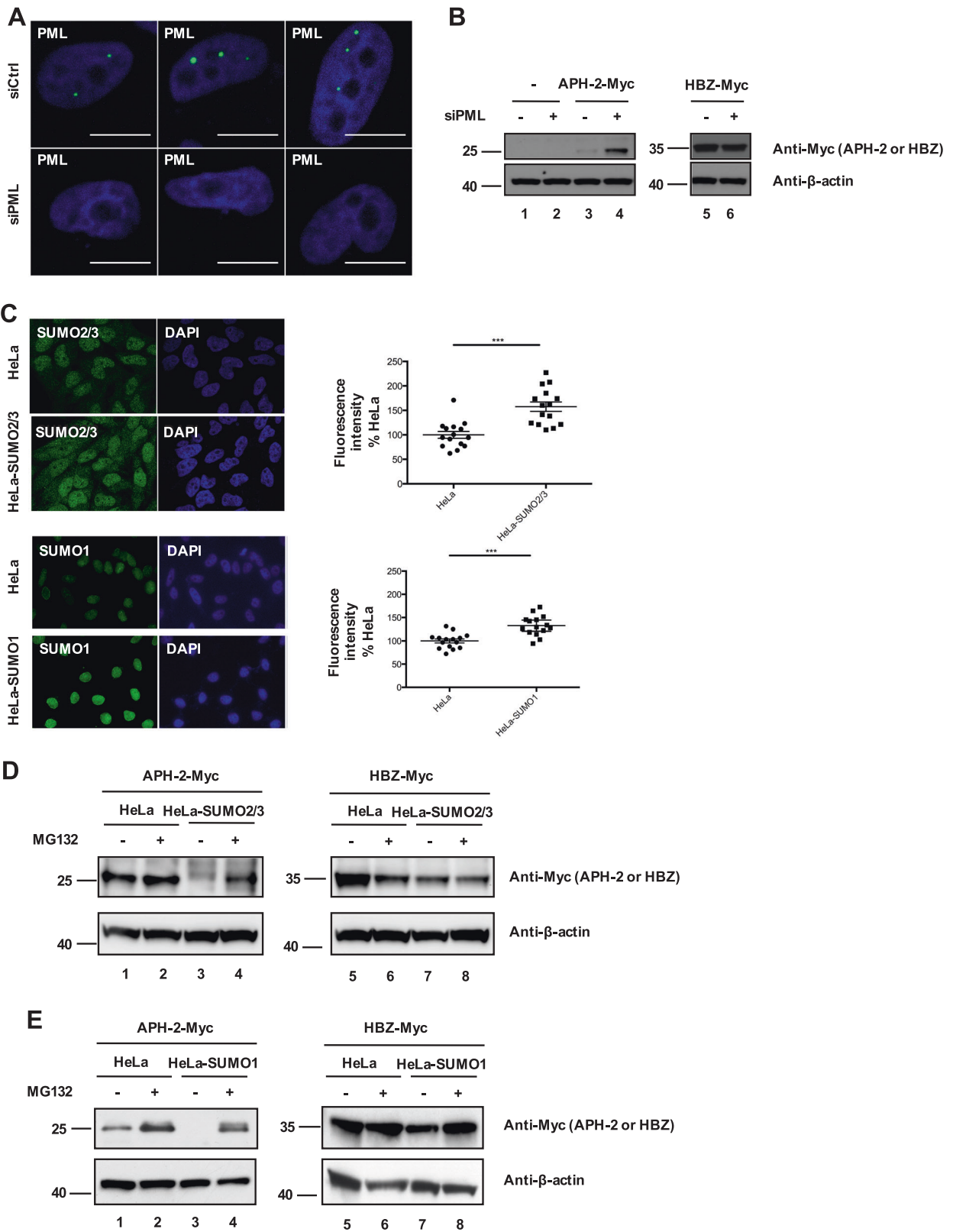


Fig. 2 The stability of APH-2 is controlled by PML nuclear bodies. **a** HeLa cells were transfected with control (siCTRL) or PML-targeting (siPML) siRNA. PML silencing was analyzed by confocal microscopy using an anti-PML antibody (green). Nuclei were counterstained with DAPI (blue). Scale bar = 10 μ m. **b** HeLa cells were transfected with HBZ-Myc or with APH-2-Myc in the presence of control (–) or PML-targeting (+) siRNA. Western blot analyses were performed using an anti-Myc antibody. Both anti-Myc panels come from the same gel but correspond to distinct exposure times. Results are representative of three independent experiments. **c** SUMO2/3 and SUMO1 expression was analyzed in HeLa, HeLa-SUMO2/3, and HeLa-SUMO1, respectively, by epifluorescence microscopy with an anti-SUMO2/3 or an anti-SUMO1 antibody (green). Nuclei were counterstained with DAPI (blue). Fluorescence intensity in 15 individual cells per condition was measured using ImageJ software and the mean intensity and SEM are plotted on the graph. ****P*-value < 0.001 (*t*-test). **d** HeLa and HeLa-SUMO2/3 or **e** HeLa and HeLa-SUMO1 cells were transfected with APH-2-Myc or HBZ-Myc and treated with MG132 (+) or vehicle (–). APH-2 and HBZ expression levels were analyzed by western blot with an anti-Myc antibody. β -actin was used as a loading control. Results are representative of at least three independent experiments

PML nuclear bodies control APH-2 stability in a SUMO-dependent manner

In order to demonstrate the involvement of PML-NBs in the control of APH-2 stability, APH-2 expression was monitored in PML-silenced cells (Fig. 2a, b). Cells were transfected with siRNA targeting PML or control siRNA, together with Myc-tagged APH-2 or HBZ constructs. First, PML silencing was validated by confocal microscopy after PML staining (Fig. 2a, see difference in cells treated with siRNA against PML or control siRNA). In PML-silenced cells, APH-2 expression levels were higher than in control cells (Fig. 2b, compare lane 4 vs. 3), indicating that indeed, PML is required for the low stability of APH-2. In contrast, HBZ expression was unaffected by PML silencing (Fig. 2b, compare lane 6 vs. 5), indicating that PML specifically controls APH-2 stability.

Because PML-NBs are enriched in SUMOylated proteins, and because SUMO modifications are known as a degradation signals for PML-NBs-associated proteins, SUMO-1 and SUMO2/3 signals were first checked by immunofluorescence and quantified in HeLa, HeLa-SUMO1, and HeLa-SUMO2/3 cells (Fig. 2c upper panel for SUMO2/3 and lower panel for SUMO1). Then, APH-2 and HBZ were transfected in HeLa-SUMO2/3 (Fig. 2d) and HeLa-SUMO1 (Fig. 2e), as well as in control HeLa cells. As compared to control HeLa cells, HeLa SUMO2/3 as well as HeLa-SUMO1 cells showed a severe decrease in APH-2 detection (Fig. 2d,e compare lanes 1 vs. 3). Proteasome inhibition by MG132 restored detection of APH-2 in HeLa-SUMO2/3 and HeLa-SUMO1 cells (Fig. 2d, e compare lanes 3 vs. 4), indicating that APH-2 is degraded by the proteasome in a SUMO-dependent manner. Of note, HBZ expression levels were unaffected by SUMO2/3 and

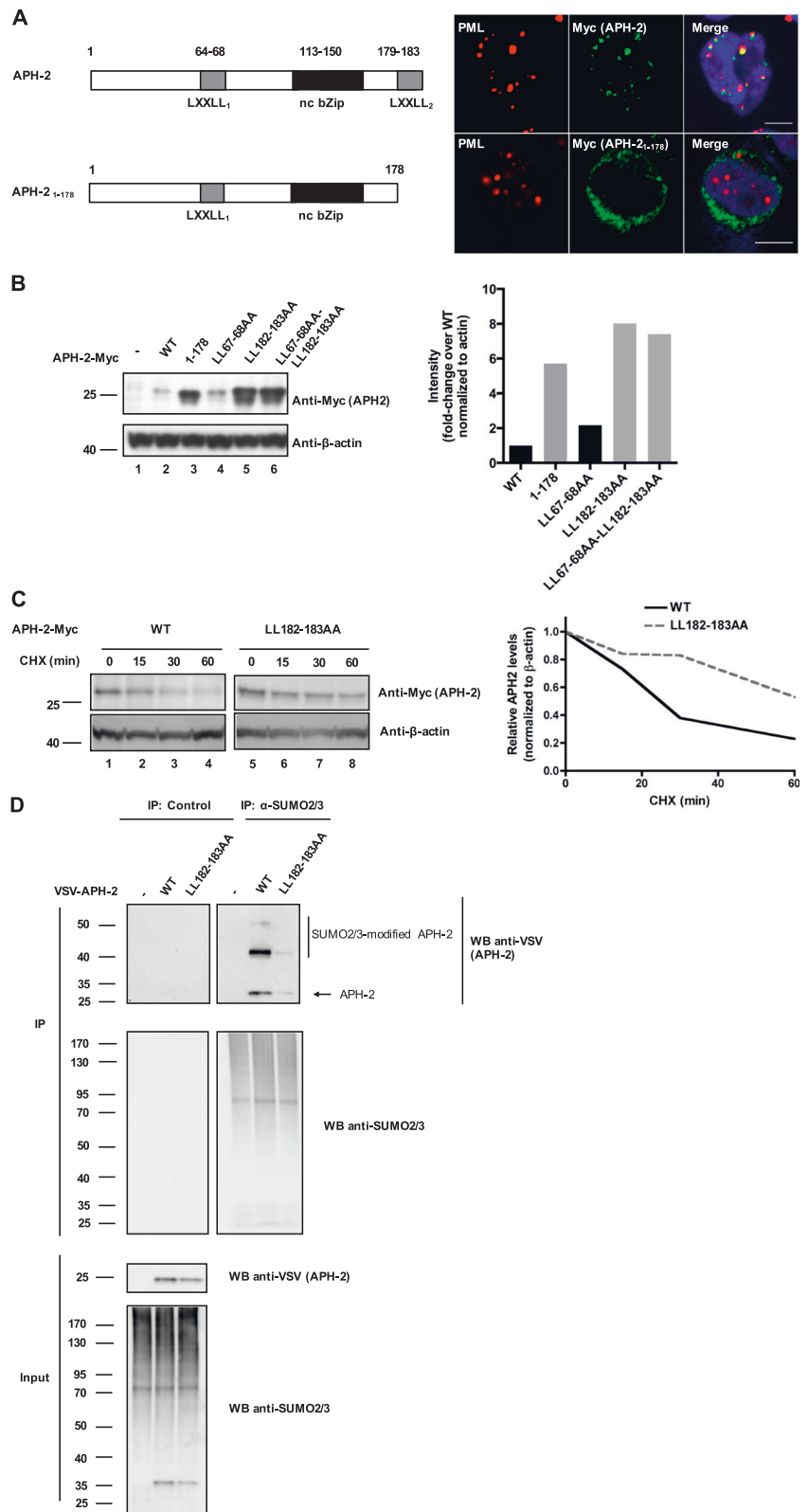
SUMO1 overexpression and only marginally affected by proteasome inhibition (Fig. 2d,e right panel), again indicating that SUMO-dependent degradation is specifically controlling APH-2 stability.

The LXXLL₂ domain of APH-2 is required for PML localization and is responsible for the short half-life of the protein

APH-2 harbors a C-terminal LXXLL motif (aa 179–183, LXXLL₂, Fig. 3a left panel) that was previously reported to be required for efficient APH-2 binding to CREB and hence for efficient repression of 5'LTR transcription by APH-2 (ref. [20]). It also harbors a LXXLL-like motif located in the central domain of the protein (aa 64–68, LXXLL₁, Fig. 3a left panel) whose function is unclear. In order to investigate whether the C-terminal LXXLL motif is involved in PML-NB localization, we generated a truncated version of the protein, APH-2_{1–178}, which lacks the C-terminal LXXLL₂ motif. Jurkat cells were transfected with full-length or truncated APH-2 and imaged by confocal microscopy after PML staining (Fig. 3a right panel). While full-length APH-2 was distributed in PML-NBs, APH-2_{1–178} was found diffuse in the cytoplasm of cells, indicating that in T-cells, the LXXLL₂ domain of APH-2 is required for nuclear localization and more specifically for PML-NBs localization. This suggests that the 179–183 motif could allow APH-2 to interact with cellular partners accumulated at PML-NBs, and hence induce its association with these nuclear subdomains. However, we could not show any accumulation of CREB in PML-NBs (data not shown), suggesting that the interaction with CREB does not mediate APH-2 association with PML-NBs.

We next used mutant APH-2 constructs to confirm that localization in PML-NBs is responsible for the short half-life of APH-2. We first analyzed the expression levels of wild-type APH-2 compared to mutant proteins that have lost the localization in PML-NBs (APH-2_{1–178}, see Fig. 3a, and APH-2_{LL182–183AA} in which the C-terminal LXXLL motif was mutated to abrogate its function). As a control, APH-2_{LL67–68AA} in which the central LXXLL-like motif was mutated, was included, as well as the APH-2_{LL67–68AA-LL182–183AA} double mutant (Fig. 3b). While WT APH-2 expression was low as usual (Fig. 3b, lane 2), expression levels of APH-2_{1–178}, APH-2_{LL182–183AA}, and APH-2_{LL67–68AA-LL182–183AA} were greatly enhanced (Fig. 3b, lanes 3, 5 and 6, see graph for quantification), demonstrating the importance of the 179–183 amino acid sequence for the control of APH2 stability. Expression levels of APH-2_{LL67–68AA} were similar to WT APH-2 (Fig. 3b, lane 4, and see graph for quantification), indicating that mutation of LXXLL-like motifs per se did not affect APH-2 stability. Thus, deletion or substitutions in the C-terminal LXXLL motif of APH-2

Fig. 3 The LXXLL₂ domain of APH-2 is required for PML localization and is responsible for the short half-life of APH-2. **a** Jurkat T-cells were transfected with full length APH-2-Myc or with APH-2₁₋₁₇₈ and fixed 24 h after transfection. Subcellular localization of APH-2 was examined by confocal microscopy after anti-Myc and anti-PML stainings. Nuclei were counterstained with DAPI (blue). Scale bar = 10 μm. Images are representative of two independent experiments. **b** HeLa cells were transfected with wild-type (WT) and mutant APH-2-Myc expression vectors. APH-2 expression levels were analyzed by western blot using an anti-Myc antibody. β-actin was used as a loading control. Signals were quantified and normalized to actin, and are shown in the graph (representative of two independent experiments). **c** HeLa cells were transfected with wild-type APH-2 or APH-2_{LL182-183AA}. Cells were treated the following day with cycloheximide for the indicated time. Immunoblot analysis was performed to monitor APH-2 expression levels. β-actin was used as a loading control. Signals were quantified and normalized to actin, and are shown on the graph (representative of two independent experiments). **d** HeLa cells were transfected with SUMO2/3 and VSV-APH-2, VSV-APH-2_{LL182-183AA} or with empty vector. After treatment with MG132, anti-SUMO2/3 immunoprecipitation was performed on cell lysates in denaturing conditions, allowing specific retention of post-translationally modified APH-2. Precipitates were analyzed by western blot using anti-SUMO2/3 and anti-VSV antibodies. Results are representative of three independent experiments. *nc bZip* non-conventional bZip domain



are sufficient to stabilize the protein, indicating that this motif is responsible for the short half-life of the protein. Because this motif is also responsible for targeting APH-2

to PML-NBs, this result is a strong additional indication that localization in PML-NBs is responsible for the short half-life of APH-2.

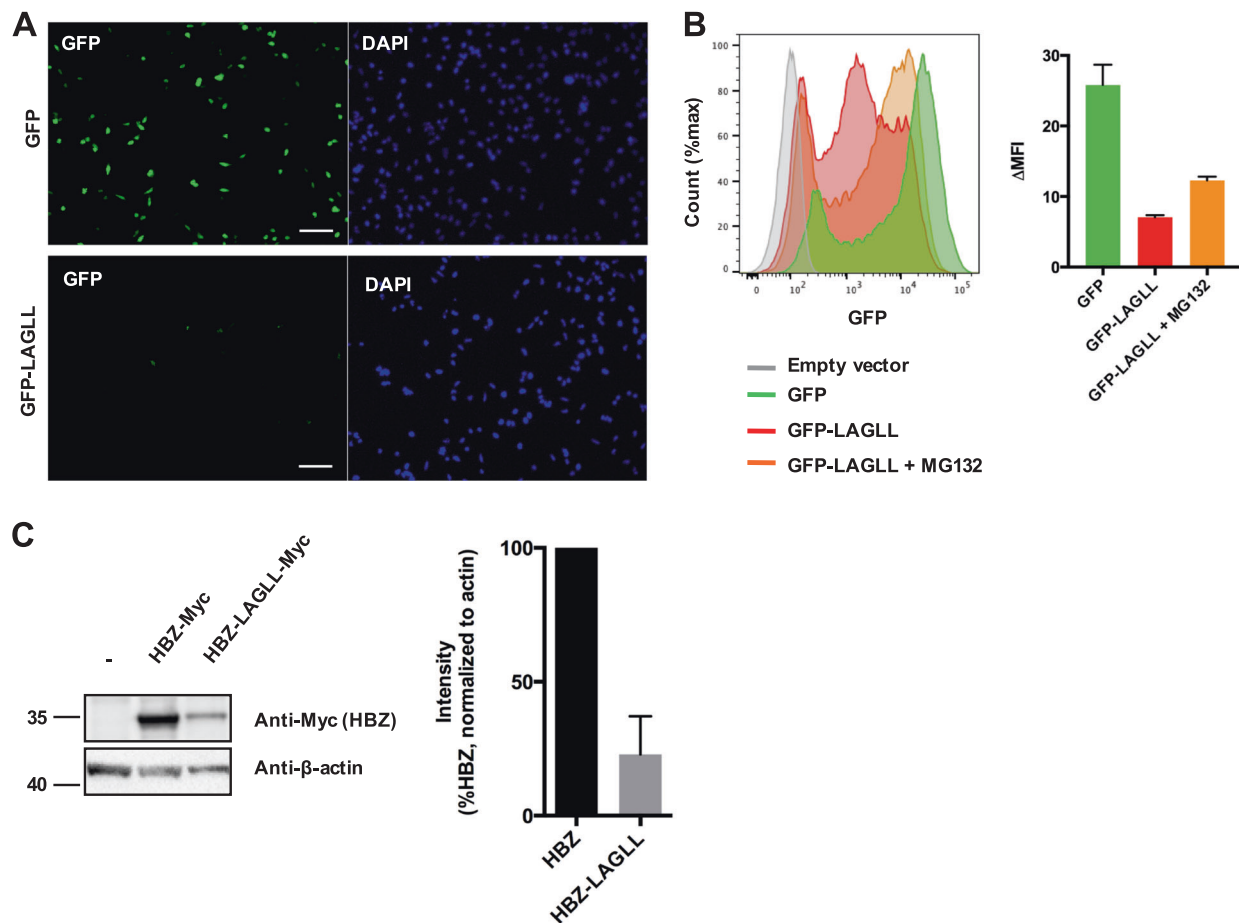


Fig. 4 The LAGLL domain of APH-2 is sufficient to induce proteasomal degradation of stable proteins. **a** HeLa cells were transfected with GFP or GFP-LAGLL constructs and fluorescence was analyzed after 24 h by epifluorescence microscopy. Nuclei were counterstained with DAPI (blue). Scale bar = 50 μ m. Images are representative of at least three independent experiments. **b** HeLa cells were transfected with GFP or GFP-LAGLL constructs and treated with MG132, when indicated. Fluorescence was analyzed by flow cytometry after 24 h following live cell gating by FCS/SSC. The gray curve represents

mock-transfected cells. Mean fluorescence intensities (MFI) are shown as Δ MFI over mock-transfected cells. The graph shows mean and SEM from three independent experiments. **c** HeLa cells were transfected with HBZ-Myc or HBZ-LAGLL-Myc expression vectors. HBZ and HBZ-LAGLL expression levels were analyzed by western blot using an anti-Myc antibody. β -actin was used as a loading control. Signals were quantified and normalized to actin, and are shown in the graph as mean and SEM from two independent experiments

To confirm that the presence of the LXXLL₂ motif of APH-2 is responsible for the short half-life of the protein, we performed cycloheximide (CHX) chase experiments (Fig. 3c). Cells were transfected with WT APH-2 or APH-2_{LL182-183AA} and treated with CHX for varying durations to inhibit protein translation. APH-2 levels were then monitored by western blot analyses. Consistent with previous reports [21], WT APH-2 levels decreased as soon as 15 min after CHX treatment. APH-2 level was reduced to 20% of initial protein amount by 60 min of treatment (Fig. 3c, see right panel for quantification). In contrast, APH-2_{LL182-183AA} levels were maintained at 80% of initial protein amount up to 30 min of treatment and reduced to 50% of initial protein amount by 60 min of treatment (Fig. 3c, right panel). This confirms that mutation of the LXXLL₂ motif of APH-2

greatly stabilizes the protein and thus that this motif contributes to the short half-life of APH-2.

Interestingly, analysis of APH-2_{LL182-183AA} SUMOylation status indicated that although SUMO2/3-modified forms remained detectable, they were markedly reduced compared to the WT APH-2 (Fig. 3d), further strengthening the conclusion that a SUMO-dependent mechanism reduces APH-2 stability.

To confirm the importance of the LXXLL₂ domain of APH-2 in the control of protein stability, this motif (which exact sequence is LAGLL) was fused at the C-terminus of either GFP or HTLV-1 HBZ (Fig. 4). Expression of GFP or GFP-LAGLL and HBZ or HBZ-LAGLL was evaluated by fluorescence microscopy (Fig. 4a), flow cytometry (Fig. 4b), and western blot (Fig. 4c), respectively. Fusion of the

LAGLL motif at the C-terminus of GFP drastically decreased its detection (Fig. 4a,b). The mean fluorescence intensity of GFP-LAGLL was ~10-fold reduced compared to GFP backbone protein alone (Fig. 4b, right panel). Of note, proteasome inhibition using MG132 partially rescued GFP-LAGLL detection (Fig. 4b), indicating that the LAGLL motif targets GFP to proteasomal degradation. It is worth noting however that GFP-LAGLL was not re-localized to PML-NBs in the presence of MG-132, suggesting that this motif is not sufficient to address GFP to PML-NBs. HBZ-LAGLL levels were also seriously reduced compared to wild-type HBZ (Fig. 4c and graph on the right for quantification of the signal). Thus, the LAGLL motif found at the C-terminus of APH-2 is sufficient to promote decreased protein stability, independently of the protein to which it is fused. Taken together, these results indicate that (i) the LAGLL motif decreases protein abundance when fused to a stable protein such as GFP, (ii) that this decrease in protein abundance is due, at least in part, to proteasomal degradation, (iii) that deletion or mutation of the LAGLL motif slows APH-2 degradation over time. These three characteristics define the LAGLL sequence in APH-2 as a degron, i.e. a sequence controlling protein degradation, in addition to its role as a PML-targeting sequence.

Taken together, these results demonstrate that APH-2 is degraded by the proteasome in a process that depends both on PML and on SUMO-1 modification. Thus, we propose that APH-2 is SUMOylated and addressed to PML-NBs before being targeted to proteasomal degradation.

Discussion

It is well established that several viruses have developed mechanisms that allow them to manipulate the cellular SUMOylation mechanisms to their profit. In general, this helps their replication and is detrimental to the infected host [23]. A substantial number of viral proteins were previously shown to be SUMOylated with either positive or negative consequence on the function of these proteins (for a review, see ref. [24]). During HTLV-1 infection, it is well established that the HTLV-1 Tax oncoprotein is SUMOylated [25], although SUMOylation does not seem to be critical for NF- κ B activation, an important step required during cell transformation [26]. Interestingly, it was demonstrated that arsenic/interferon combination which is used to treat ATLL patients, leads to HTLV-1 Tax poly-SUMOylation followed by degradation in PML nuclear bodies [27]. SUMO also contributes to the anti-HIV-1 effect of interferon [28]. HTLV-2 is barely pathogenic, and on the contrary to HTLV-1 Tax, its Tax protein is barely SUMOylated [29].

As HTLV-1, which encodes HBZ, HTLV-2 infection leads to transcription of the antisense protein of HTLV-2 (*aph-2*) mRNA that is expressed in vivo in most HTLV-2 carriers. APH-2 protein is barely detectable in vitro with a half-life of 20 min in T-cells, and this short half-life is mainly due to a low protein stability [21]. The lack of ability of APH-2 to enhance TGF- β signaling, or to repress NF- κ B p65 or IRF-1 transactivation [21] might be due to the very low availability of the protein in cells.

A number of previously published studies demonstrated that the replication of some DNA viruses is targeted by PML-NBs (for a review see ref. [30]). Here, our results show that APH-2 is very efficiently addressed to PML-NBs. However, the situation is distinct from DNA viruses, since APH-2 is absent from the viral particle, thus its expression requires productive infection. We have demonstrated here that the C-terminal LXXLL domain of APH-2 is required for the efficient localization of the protein to PML-NBs. Interestingly, this motif represents a protein-protein interaction motif that was previously identified as necessary for APH-2 interaction with CREB [20]. However, we excluded the possibility that CREB mediated the recruitment of APH-2 in PML-NBs. The “LAGLL” sequence was also identified as a Sin3a-interacting motif in the Sin3a-associated protein SAP25 (ref. [31]), raising the possibility that APH-2 could also interact with Sin3a. Sin3a is a transcriptional modulator that interacts with multiple partners including transcriptional repressors, enzymes that perform post-translational modifications, DNA binding factors and docking proteins (for a review, see [32]). Sin3a is also able to maintain HIV-1 replication at a latency stage [33]. Because SAP25 was shown to concentrate in PML-NBs, it has been postulated that SAP25 could address the Sin3a complex to PML-NBs [31], a hypothesis consistent with the observation that Sin3a interacts with PML [34]. Interestingly, we observed that APH-2 interacts with Sin3a, although its LAGLL motif is dispensable for the interaction (data not shown). Thus, whether APH-2 interferes with the PML-dependent activities of the Sin3a complex is under current investigation. Altogether, these observations indicate that APH-2 could both be controlled by PML-dependent processes, but also modulate PML-dependent cellular activities, such as transcriptional regulation.

We previously showed that HTLV-2 neo-infection is very sensitive to type I interferon (IFN-I) [35]. Because PML is an IFN-I-induced gene product that was shown to mediate the IFN-I-induced antiviral state against human retroviruses such as human foamy virus [36], it is possible to hypothesize that PML has two functions during HTLV-2 infection: (1) inducing APH-2 degradation and (2) being involved in the IFN-induced antiretroviral defense mechanism.

Materials and methods

Cell culture

HeLa and Jurkat T cells were obtained from the American type culture collection (ATCC). HeLa cells stably expressing SUMO-1 (HeLa-SUMO-1) and parental HeLa cells were described elsewhere [37]. HeLa cells and stable HeLa-SUMO1 cells were maintained in high glucose, GlutaMAX Dulbecco's modified Eagle's medium (DMEM, Gibco, Life Technologies) supplemented with 10% fetal bovine serum (FBS, Biosera) and antibiotics (100 U/ml penicillin and 100 µg/ml streptomycin, Gibco, Life Technologies). Jurkat cells were maintained in GlutaMAX Roswell Park Memorial Institute medium (RPMI, Gibco, Life Technologies) supplemented with 10% FBS and antibiotics (100 U/ml penicillin and 100 µg/ml streptomycin, Gibco, Life Technologies). All cells were maintained at 37 °C in 5% CO₂ and tested for mycoplasma contamination at regular intervals.

Plasmids and siRNA

pcDNA3.1-APH2-Myc-His and pcDNA3.1-HBZ-Myc-His expression vectors [18, 38], as well as HA-SUMO1 and HA-SUMO3 expression vectors were previously described [25]. APH2 truncation mutant (APH2₁₋₁₇₈) as well as HBZ-LAGLL fusion protein were PCR-amplified and cloned between EcoRI and HindIII sites into the pcDNA3.1-Myc-His vector (Promega). The LAGLL peptide sequence was inserted downstream the GFP coding sequence by primer hybridization and cloning between the EcoRI and BamHI sites of the pEGFP-C3 vector (Clontech). Expression vectors for mutated APH2-LXXAA₁ (⁶⁷LL⁶⁸ to ⁶⁷AA⁶⁸), APH2-LXXAA₂ (¹⁸²LL¹⁸³ to ¹⁸²AA¹⁸³), and APH2-LXXAA₁₋₂ (combining mutations in both LXXLL motifs) were obtained using the QuikChange II site-directed mutagenesis kit (Stratagene) and verified by Sanger sequencing (GATC).

The following siRNAs directed against PML were used: 5' CACCCGCAAGACCAACAACA3' and 5' GUGUACCGGCAGAUUGUGGAU3' (Sigma-Aldrich).

Antibodies

The following primary antibodies were used: mouse anti-PML (sc-966, Santa Cruz Biotechnology); mouse anti-Myc (clone 4A6, Merck Millipore); FITC-labeled mouse anti-Myc (clone 9E10, Sigma); mouse anti-β-actin (clone AC-74, Sigma-Aldrich); anti-GMP-1/SUMO-1 (clone 21C7, Invitrogen), mouse anti-VSV (clone P5D4, Sigma-Aldrich); rabbit anti-VSV (V4888, Sigma-Aldrich); rabbit anti-SUMO2/3 (ab3742, Abcam), anti-SUMO2/3-HRP (from Signal-Seeker™ SUMOylation 2/3 Detection Kit,

Cytoskeleton), rabbit anti-His (sc-804, Santa Cruz). The following secondary antibodies were used in western blot: horseradish peroxidase-conjugated anti-mouse IgG (NA9310, GE Healthcare or #32430, Thermo Fisher) and anti-rabbit IgG (NA9340, GE Healthcare or #32460, Thermo Fisher).

Transient transfections

For western blot, immunoprecipitation and immunofluorescence assays, HeLa cells were transiently transfected using Effectene or Polyfect transfection reagents (Qiagen), according to the manufacturer's guidelines. For siRNA experiments, 2 × 10⁵ HeLa cells were seeded in six-well plates and transfected the following day with 50 pmol of siPML using Lipofectamine 2000 Reagent (Life Technology).

Jurkat cells were transfected by electroporation with Neon Transfection kit (MPK5000, Invitrogen). Briefly, 4 × 10⁵ cells were electroporated with 2 µg of DNA using a 10 µl tip (MPK1096, Invitrogen). Electroporation conditions were: voltage 1325 V, 3 pulsations of 10 ms. Cells were maintained in antibiotic-free RPMI containing 10% FBS for 24 h post-transfection and seeded on poly-lysine-coated coverslips for immunofluorescence assays.

Cycloheximide analysis

Sixteen hours post-transfection, cells were incubated in the presence of cycloheximide (CHX, 100 µg/ml) for varying durations before harvesting and western blot analysis. Results are representative of two independent experiments.

Proteasome inhibition

Twenty-four hours post-transfection, HeLa and stable HeLa-SUMO-1 cells were treated with 10 µM of the proteasome inhibitor MG-132 (Calbiochem) for 16 h at 37 °C. DMSO was used as a vehicle.

Fluorescence microscopy

Cells seeded on coverslips were fixed 24 h after transfection with formalin (HT5011, Sigma-Aldrich) for 20 min. Cells were washed in PBS and permeabilized in PBS-Triton X-100 0.5% for 30 min at room temperature. Cells were then washed, saturated in PBS-Tween 0.2%–milk 5% for 1 h and incubated for 45 min with primary antibodies in saturation buffer. Cells were then washed and incubated for 45 min with the appropriate conjugated secondary antibodies prepared in saturation buffer. Coverslips were mounted in mounting medium containing DAPI (Fluoromount-G, 0100-20, Southern Biotech).

For confocal analyses, slides were examined under a Leica spectral SP5 confocal microscope equipped with a 63× 1.4–0.6 oil-immersion objective using the LAS-AF software, or under an inverted confocal microscope (LSM 800; Carl Zeiss MicroImaging) equipped with a 63× 1.4 plan apochromat oil-immersion objective on the ZEN software and analyzed using the ImageJ software. Images representative of at least two independent experiments are shown.

For epifluorescence imaging, slides were examined under an AxioImager.Z1 microscope (Zeiss) equipped with a 63×/1.4 Plan Apochromat oil-immersion objective. Images were acquired using a Coolsnap HQ monochrome CCD (Zeiss; 1392 × 1040–6.45 μm pixel; 12 bit) camera and the MetaMorph software. Fluorescence intensity was measured in 15 cells/condition using ImageJ software and Student's *t*-test was used to compare means. GFP epifluorescence was analyzed under an AMG Evos fl digital inverted fluorescence microscope. Images are representative of at least three independent experiments.

Flow cytometry analyses

Cells were fixed in 4% paraformaldehyde and analyzed on a MACSQuant cytometer (Miltenyi) in three independent experiments. FACS analyses were performed under the FlowJo software.

Western blots

Cells were lysed in radioimmunoprecipitation assay (RIPA) buffer containing 50 mM Tris–HCl pH 7.4, 150 mM NaCl, 1% Nonidet P-40, 0.25% Na-Doc, 5 mM PMSF, and protease inhibitors (Complete Protease Inhibitor Cocktail EDTA-free, Roche) at 4 °C for 20 min. After centrifugation and protein concentration determination (Bradford, Biorad), lysates were separated by SDS-PAGE on Criterion XT precast gels 10% Bis–Tris (Biorad) or on NuPAGE Novex 4–12% Bis–Tris Gel (Invitrogen), transferred on PVDF membrane and saturated in TBS–Tween 0.1%–milk 5%. After incubation with the appropriate primary and secondary antibodies, ECL prime western blotting detection reagent (GE healthcare) and super signal west femto maximum sensitivity substrate (Thermo Scientific) were used for revelation. Signals were quantified with ImageJ software.

Denaturing immunoprecipitation

To examine covalent protein–protein interaction between APH2 and SUMO-2/3, HeLa cells were treated with 10 μM MG-132 for 16 h before lysis and immunoprecipitation of SUMO2/3 using the Signal-Seeker™

SUMOylation 2/3 Detection Kit (Cytoskeleton) according to the manufacturer's instructions. Briefly, three 100 mm dishes of HeLa cells were harvested in lysis buffer. After protein quantification, 1.2 mg of proteins were incubated with control beads or SUMO2/3 affinity beads 2 h at 4 °C. After wash, proteins were eluted and analyzed by western blot together with whole cell extracts (input). Results are representative of three independent experiments.

To examine covalent protein–protein interaction between APH-2 and SUMO1, HeLa cells were treated with 10 μM MG-132 for 16 h before lysis in Abis–Guanidine buffer (Guanidine 6 M, NaH₂PO₄ 100 mM, imidazole 10 mM). After sonication, proteins were incubated with Ni-NTA beads (His-select HF Agarose Beads, Sigma-Aldrich) overnight at 4 °C. Bound fractions were then washed three times in Abis–Guanidine buffer, twice in 0.25× Abis–Guanidine buffer (diluted in Tris–HCl 25 mM, imidazole 10 mM), and twice in Tris–HCl 25 mM, imidazole 10 mM, before elution in Laemmli buffer followed by western blot analysis. Results are representative of two independent experiments.

Statistical analyses

No specific test was used to calculate the sample size. When appropriate, unpaired two-sided Student's *t*-test with Welch's correction was used (GraphPad Prism) to compare means of two experimental groups for which data followed a normal distribution.

Acknowledgements We thank the microscopy facility team of the Lyon SFR Biosciences. R.M., C.J., and F.L. are supported by ENS Lyon. L.D. is supported by ANR. J.T. was supported by the Fondation ARC pour la Recherche sur le Cancer. E.D. was supported by the Ministère de la Recherche. This work was supported by ARC and La Ligue Contre le Cancer “programme Équipe Labellisée” and INSERM.

Compliance with ethical standards

Conflict of interest The authors declare that they have no conflict of interest.

References

1. Bruhn RMR. Human lymphotropic viruses: HTLV-1 and HTLV-2. In: Richman DWR, editor. Clinical virology. 4th ed. Washington, DC: AM Press; 2017. p. 771–94.
2. Ciminale V, Rende F, Bertazzoni U, Romanelli MG. HTLV-1 and HTLV-2: highly similar viruses with distinct oncogenic properties. *Front Microbiol.* 2014;5:398.
3. Wang TG, Ye J, Lairmore MD, Green PL. In vitro cellular tropism of human T cell leukemia virus type 2. *AIDS Res Hum Retrovir.* 2000;16:1661–8.
4. Xie L, Green PL. Envelope is a major viral determinant of the distinct in vitro cellular transformation tropism of human T-cell

- leukemia virus type 1 (HTLV-1) and HTLV-2. *J Virol.* 2005;79:14536–45.
5. Curren R, Van Duyne R, Jaworski E, Guendel I, Sampey G, Das R, et al. HTLV tax: a fascinating multifunctional co-regulator of viral and cellular pathways. *Front Microbiol.* 2012;3:406.
 6. Zhao T, Matsuoka M. HBZ and its roles in HTLV-1 oncogenesis. *Front Microbiol.* 2012;3:247.
 7. Mesnard JM, Barbeau B, Cesaire R, Peloponese JM. Roles of HTLV-1 basic Zip factor (HBZ) in viral chronicity and leukemic transformation. potential new therapeutic approaches to prevent and treat HTLV-1-related diseases. *Viruses.* 2015;7:6490–505.
 8. Journo C, Douceron E, Mahieux R. HTLV gene regulation: because size matters, transcription is not enough. *Future Microbiol.* 2009;4:425–40.
 9. Kfoury Y, Nasr R, Journo C, Mahieux R, Pique C, Bazarbachi A. The multifaceted oncoprotein Tax: subcellular localization, post-translational modifications, and NF-kappaB activation. *Adv Cancer Res.* 2012;113:85–120.
 10. Watanabe T. Adult T-cell leukemia: molecular basis for clonal expansion and transformation of HTLV-1-infected T cells. *Blood.* 2017;129:1071–81.
 11. Yamano Y, Sato T. Clinical pathophysiology of human T-lymphotropic virus-type 1-associated myelopathy/tropical spastic paraparesis. *Front Microbiol.* 2012;3:389.
 12. Gaudray G, Gachon F, Basbous J, Biard-Piechaczyk M, Devaux C, Mesnard JM. The complementary strand of the human T-cell leukemia virus type 1 RNA genome encodes a bZIP transcription factor that down-regulates viral transcription. *J Virol.* 2002;76:12813–22.
 13. Satou Y, Yasunaga J, Zhao T, Yoshida M, Miyazato P, Takai K, et al. HTLV-1 bZIP factor induces T-cell lymphoma and systemic inflammation in vivo. *PLoS Pathog.* 2011;7:e1001274.
 14. Giam CZ, Semmes OJ. HTLV-1 infection and adult T-cell leukemia/lymphoma-A tale of two proteins: Tax and HBZ. *Viruses.* 2016;8:E161. <https://doi.org/10.3390/v8060161>.
 15. Nicot C. HTLV-I Tax-mediated inactivation of cell cycle checkpoints and DNA repair pathways contribute to cellular transformation: 'A Random Mutagenesis Model'. *J Cancer Sci* 2015; 2. <https://doi.org/10.13188/2377-9292.1000009>.
 16. Shirinian M, Kambris Z, Hamadeh L, Grabbe C, Journo C, Mahieux R, et al. A transgenic *Drosophila melanogaster* model to study human T-lymphotropic virus oncoprotein Tax-1-driven transformation in vivo. *J Virol.* 2015;89:8092–5.
 17. El Hajj H, El-Sabban M, Hasegawa H, Zaatari G, Ablain J, Saab ST, et al. Therapy-induced selective loss of leukemia-initiating activity in murine adult T cell leukemia. *J Exp Med.* 2010;207:2785–92.
 18. Halin M, Douceron E, Clerc I, Journo C, Ko NL, Landry S, et al. Human T-cell leukemia virus type 2 produces a spliced antisense transcript encoding a protein that lacks a classic bZIP domain but still inhibits Tax2-mediated transcription. *Blood.* 2009;114:2427–38.
 19. Douceron E, Kaidarova Z, Miyazato P, Matsuoka M, Murphy EL, Mahieux R. HTLV-2 APH-2 expression is correlated with proviral load but APH-2 does not promote lymphocytosis. *J Infect Dis.* 2012;205:82–6.
 20. Yin H, Kannian P, Dissinger N, Haines R, Niewiesk S, Green PL. Human T-cell leukemia virus type 2 antisense viral protein 2 is dispensable for in vitro immortalization but functions to repress early virus replication in vivo. *J Virol.* 2012;86:8412–21.
 21. Panfil AR, Dissinger NJ, Howard CM, Murphy BM, Landes K, Fernandez SA, et al. Functional comparison of HBZ and the related APH-2 protein provides insight into human T-cell leukemia virus type 1 pathogenesis. *J Virol.* 2016;90:3760–72.
 22. Hivin P, Basbous J, Raymond F, Henaff D, Arpin-Andre C, Robert-Hebmann V, et al. The HBZ-SP1 isoform of human T-cell leukemia virus type I represses JunB activity by sequestration into nuclear bodies. *Retrovirology.* 2007;4:14.
 23. Lowrey AJ, Cramblet W, Bentz GL. Viral manipulation of the cellular sumoylation machinery. *Cell Commun Signal.* 2017;15:27.
 24. Everett RD, Boutell C, Hale BG. Interplay between viruses and host sumoylation pathways. *Nat Rev Microbiol.* 2013;11:400–11.
 25. Nasr R, Chiari E, El-Sabban M, Mahieux R, Kfoury Y, Abdulhay M, et al. Tax ubiquitylation and sumoylation control critical cytoplasmic and nuclear steps of NF-kappaB activation. *Blood.* 2006;107:4021–9.
 26. Pene S, Waast L, Bonnet A, Benit L, Pique C. A non-SUMOylated tax protein is still functional for NF-kappaB pathway activation. *J Virol.* 2014;88:10655–61.
 27. Dassouki Z, Sahin U, El Hajj H, Jollivet F, Kfoury Y, Lallemand-Breitenbach V, et al. ATL response to arsenic/interferon therapy is triggered by SUMO/PML/RNF4-dependent Tax degradation. *Blood.* 2015;125:474–82.
 28. Sahin U, Ferhi O, Carnec X, Zamborlini A, Peres L, Jollivet F, et al. Interferon controls SUMO availability via the Lin28 and let-7 axis to impede virus replication. *Nat Commun.* 2014;5:4187.
 29. Journo C, Bonnet A, Favre-Bonvin A, Turpin J, Vinera J, Cote E, et al. Human T cell leukemia virus type 2 tax-mediated NF-kappaB activation involves a mechanism independent of Tax conjugation to ubiquitin and SUMO. *J Virol.* 2013;87:1123–36.
 30. Komatsu T, Nagata K, Wodrich H. The role of nuclear antiviral factors against invading DNA viruses: the immediate fate of incoming viral genomes. *Viruses.* 2016;8:E290. <https://doi.org/10.3390/v8100290>.
 31. Shiio Y, Rose DW, Aur R, Donohoe S, Aebersold R, Eisenman RN. Identification and characterization of SAP25, a novel component of the mSin3 corepressor complex. *Mol Cell Biol.* 2006;26:1386–97.
 32. Kadamb R, Mittal S, Bansal N, Batra H, Saluja D. Sin3: insight into its transcription regulatory functions. *Eur J Cell Biol.* 2013;92:237–46.
 33. Jean MJ, Power D, Kong W, Huang H, Santoso N, Zhu J. Identification of HIV-1 Tat-associated proteins contributing to HIV-1 transcription and latency. *Viruses.* 2017;9:E67. <https://doi.org/10.3390/v9040067>.
 34. Khan MM, Nomura T, Kim H, Kaul SC, Wadhwa R, Shinagawa T, et al. Role of PML and PML-RARalpha in Mad-mediated transcriptional repression. *Mol Cell.* 2001;7:1233–43.
 35. Cachat A, Chevalier SA, Alais S, Ko NL, Ratner L, Journo C, et al. Alpha interferon restricts human T-lymphotropic virus type 1 and 2 de novo infection through PKR activation. *J Virol.* 2013;87:13386–96.
 36. Regad T, Saib A, Lallemand-Breitenbach V, Pandolfi PP, de The H, Chelbi-Alix MK. PML mediates the interferon-induced antiviral state against a complex retrovirus via its association with the viral transactivator. *EMBO J.* 2001;20:3495–505.
 37. Ivanschitz L, Takahashi Y, Jollivet F, Ayrault O, Le Bras M, de The H. PML IV/ARF interaction enhances p53 SUMO-1 conjugation, activation, and senescence. *Proc Natl Acad Sci USA.* 2015;112:14278–83.
 38. Thebault S, Basbous J, Hivin P, Devaux C, Mesnard JM. HBZ interacts with JunD and stimulates its transcriptional activity. *FEBS Lett.* 2004;562:165–70.